Preprint Title	The effects of silver nanoparticles (AgNPs) on thermophilic bacteria: Antibacterial, morphological, physiological and biochemical investigations
Authors	Israt Jahan, Fatma Matpan Bekler, Ahmed Tunç and Kemal Güven
Publication Date	05 Sep. 2023
Article Type	Full Research Paper
ORCID® iDs	Israt Jahan - https://orcid.org/0000-0003-4166-1617; Fatma Matpan Bekler - https://orcid.org/0000-0001-8253-9568; Ahmed Tunç - https://orcid.org/0000-0001-6552-2211; Kemal Güven - https://orcid.org/0000-0002-0181-3746

The effects of silver nanoparticles (AgNPs) on thermophilic bacteria: Antibacterial, morphological, physiological and biochemical investigations

Israt Jahan[‡1], Fatma Matpan Bekler [‡2], Ahmed Tunç [‡3], Kemal Güven[‡*2]

Address: [1] Department of Health Care Services, Vocational School of Health Services Mardin Artuklu University, Mardin, Türkiye; sonia.israt2@gmail.com

[2] Department of Molecular Biology and Genetics, Faculty of Science, Dicle University, Diyarbakir-Türkiye; fmatpan@dicle.edu.tr, kemalg@dicle.edu.tr

[3] Department of Interdisciplinary Nanotechnology, Graduate School of Natural and Applied Sciences, Dicle University, Diyarbakir-Türkiye; ahmedtunc505@gmail.com,

Email: Kemal Güven - kemalg@dicle.edu.tr

* Corresponding author

‡ Equal contributors

Abstract

Since thermophilic microorganisms are valuable source of thermostable enzymes, it is essential to recognize the potential toxicity of silver nanoparticles used in diverse industrial sectors. Thermophilic bacteria *Geobacillus vulcani* 2Cx, *Bacillus licheniformis* 3CA, *Paenibacillus macerans* 3CA1, *Anoxybacillus ayderensis* FMB1, and *Bacillus paralicheniformis* FMB2-1 were selected, and their MIC and MBC values were assessed by treating with AgNPs at a range of 62.5-1500 µg mL^{-1}. The growth inhibition curves showed that *G. vulcani* 2Cx, and *B. paralicheniformis* FMB2-1 strains were more sensitive to AgNPs, demonstrating a reduction in population by 71.1% and 31.7% at 62.5 µg mL^{-1} and by 82.9% and 72.8% at 250 µg mL^{-1}, respectively. TEM and FT-IR analysis revealed that AgNPs caused structural damage, cytoplasmic leakage, and disruption of cellular integrity. Furthermore, the cell viability showed a significant decrease alongside an increase in superoxide radicals (SOR; O2·−) production. The β-galactosidase biosynthesis decreased to 28.8% levels at 500 µg mL^{-1} AgNPs for *G. vulcani* 2Cx, 32.2% at 250 µg mL^{-1} for *A. ayderensis* FMB1, 38.8% only at 62.5 µg mL^{-1} but completely inhibited at 500 µg mL^{-1} for *B. licheniformis* 3CA. Moreover, *B. paralicheniformis* FMB2-1 showed significant decrease to 11.2% at 125 µg mL^{-1}. This study is the first to reveal the toxic effects of AgNPs on thermophilic bacteria.

Keywords

Introduction

Over the past two decades, there has been a notable surge in industrial engagement with nanoscience and the manufacturing of nanotech-integrated items [1]. Within the United States for instance, a significant proportion (94%) of nano-scaled components dis-charged into the natural ecosystem through the application of cosmetics and personal grooming items predominantly comprises silver (1.2–272 t/year), titanium dioxide (870–1000 t/year) and zinc oxide (1800–2100 t/year) [2,3]. This excessive generation, applica-tion, and improper handling of nano-sized substances have expedited their release into multiple ecological domains, which may led to potential environmental contamination. Hence, ongoing research continues to explore the potential implications of nanoparticles on both human health and the ecosystem, underscoring their potential impact. [4] The term "nanoparticle" refers to a comprehensive range of elements that encompass particu-late substances with the lowest extent of one dimension measuring less than 100 nm [5] They have found applications across diverse fields, spanning medicine, biological science, electronics, agricultural and environmental science, and energy [6]. Their small size facil-itates penetration of biological barriers and targeted delivery to specific sites within the body, thereby enhancing the efficiency and effectiveness of therapeutic or other biological interventions [7].

Compared to other nanomaterials, silver nanoparticles (AgNPs) have received substantial recognition because of their distinctive properties [8]. Specially, the reason to gain much attention, AgNPs have found widespread application across diverse fields, such as household, industrial and consumer goods, cosmetics, textiles, food processing and packaging, pharmaceuticals, medical devices, diagnostics, orthopedics, drug delivery, wound dressings, and the development of antibacterial and anticancer agents [9,10], as well as in preventing biofilm formation and inhibiting the growth of pathogens on catheters, cardiovascular implants, and bone implants, offering promising avenues for treatment [11,12]. As the utilization of AgNPs continues to expand, it becomes increasingly imperative to acquire a deeper comprehension of their toxicity and the underlying mechanisms involved.

Nanoparticles (NPs) are increasingly used to target both Gram-negative and Gram-positive bacteria, alone or in combination with antibiotics to combat multidrug resistance in pathogenic bacteria due to broad-spectrum antibacterial properties [13]. The antibacterial impact of AgNPs is considered to be due to their smaller particles size which has an efficient penetration ability into bacterial cells, particularly in Gram-negative [14]. The antibacterial effect of AgNPs is also concentration-dependent [15]. In general, it is well studied that the size of nanoparticles should be smaller than 50 nm to be effective for en-hanced antimicrobial activity [16]. In addition, the shapes of the nanoparticles also show different effects on the interaction, so it has been reported that spherical nanoparticles with a larger effective specific contact area cause more damage than rod-shaped or wire-shaped nanoparticles by making closer contact with the bacterial cell [17,18].

In many studies carried out recently have revealed that microbial activity rates resulting in a decrease in microbial population and diversity, particularly in the soil microbial biomass, including nitrogen fixing and ammonia-oxidizing microorganisms [19-24]. While certain studies have posited that the toxicity of AgNPs primarily stems from the re-lease of Ag+ ions, which readily infiltrate bacterial cells, resulting in cellular damage and the inhibition of essential functions, other factors may also contribute to the observed toxicity [25]. Metal ions, when released gradually from NPs and absorbed onto the cell mem-brane, directly interact with functional groups (such as mercapto, amino, and carboxyl groups) found in nucleic acids and proteins. These interactions lead to enzyme activity impairment, changes in cell structure, disruptions in normal physiological processes, and ultimately the inhibition of microorganisms [26]. Moreover, numerous studies has consistently demonstrated that the toxicity of AgNPs primarily stems from their direct inter-action with functional groups present on the cell surface, which is subsequently followed by internalization into the cells. This interaction causes detrimental effects such as mem-brane damage, oxidative stress, and significant mortality [14,27].

Extensive research has been documented in the literature, exploring the effects of diverse nanoparticles (NPs) on enzyme activity in microorganisms, animals, and plants [28-33]. In particular, biochemical, physiological and molecular effects have been investigated in different soil organisms and microorganisms. AgNPs have been demonstrated to inhibit the activity of numerous extracellular enzymes, such as urease, phosphatase, phosphomonoesterase, β-D-glucosidase, leucine-aminopeptidase and arylsulfatase. This inhibition can be attributed to the binding of released Ag+ ions to thiol groups of enzymes or the direct interaction between AgNPs and the enzymes, potentially altering their con-formation or obstructing the active site [27, 34]. Unlike certain small molecules and bio-logical molecules, metallic nanoparticles (NPs) exhibit a notable propensity for easy cellular entry [35]. Additionally, metallic nanoparticles (NPs) engage with essential components within bacterial cells, such as ribosomes, enzymes, and DNA, inducing protein de-activation, enzyme inhibition, and modulation of gene expression [36,37].

Thermophilic bacteria primarily thrive in hot springs, enduring and adapting to temperatures ranging from 40 to 120 °C. They possess physically and chemically stable enzymes with unique macromolecular properties, allowing them to thrive at high temperatures and achieve higher end product yields compared to mesophilic bacteria. Thermophilic microorganisms have raised a special interest and demand for past few years as a source of novel thermostable enzymes having applications particularly in sugar industry and starch processing, production of low lactose milk, alcohol production, in the fruit, paper and leather industries, and in laundry detergents [38-42]. The unique structure of cell wall and mechanisms of their adaptation also makes thermophilics appropriate candidates for bioremediation of metals from environments or for remediation of textile dyes [42, 43-46]. The Bacillus genus and its respective species are highly valued in the en-zyme and pharmaceutical industries, thanks to their significant presence of potential bio-active compounds [12]. As thermophilic microorganisms play a crucial role in the pro-duction of thermostable enzymes like β-galactosidase [47,51], there is a lack of comprehensive understanding regarding the antibacterial mechanisms of AgNPs and the factors that impact enzyme biosynthesis, secretion, and inhibition. Thus, a detailed elucidation of these aspects is essential.

This study therefore is specifically designed to explore the effects of different concentrations of AgNPs on the structural integrity and vital functions of thermophilic bacteria, which include (i) assessing the susceptibility of bacterial strains and their growth under AgNP-induced stress, (ii) evaluating changes in cell morphology, (iii) detecting AgNP interaction with bacterial biomasses through FT-IR analysis, (iv) examining the toxic effects on cellular respiration, (v) measuring superoxide production, and (vi) investigating the inhibition of enzyme biosynthesis and extracellular secretion under AgNP-induced stress.

Materials and Methods

Silver Nanoparticles (AgNPs)

AgNPs were obtained commercially from chemPUR (Germany) and physicochemical

characteristics are shown in Table 1.

Table 1. Characteristics of silver (Ag) nanoparticles

AgNP Characteristics	
Purity	99.5%(metal basis)
Average particle size	35nm
Specific surface area	20-30 m^2/g
Particle morphology	spherical
Appearance	grey powder

Determination of Silver (Ag) Ion Release from AgNPs

To determine the effect of the utilized basal medium on 250 μg mL^{-1} concentrations of

AgNPs, the samples were kept on shaking incubator (at 100 rpm for 24 h) and metal

ion release from AgNPs was measured by FAAS (PinAAcle 500 Flame Atomic

Absorption Spectrometer, PerkinElmer), following the modified method described by

Dong et al., [52].

Strains and Maintenance of Cultures

The strains used in the present study were *Geobacillus vulcani* 2Cx (GenBank

accession number: MT350132), *Bacillus licheniformis* 3CA (GenBank accession

number: MT350128) and *Paenibacillus macerans* 3CA1 (GenBank accession number:

MT350131) isolated and identified from Diyarbakır Çermik hot water spring (38° 8'

27.2544'' N, 39° 28' 46.6068'' E) [53], *Anoxybacillus ayderensis* FMB1 (GenBank

accession number: KP992869) [54] and *Bacillus paralicheniformis* FMB2-1 (GenBank

accession number: KP992870) [55] isolated and identified from Yozgat Sorgun hot water spring (39° 48' 14.0718" N, 35° 12' 31.0752" E).

All stock bacterial strains were first introduced into Nutrient Broth (NB), which served as the growth medium. The inoculated bacterial cultures were placed in a water bath shaker set at 50 °C for a duration between 12 to 24 hours to allow the bacteria to grow. After the incubation period, the bacterial cultures were subjected to centrifugation at room temperature and a speed of 10000 rpm for 10 minutes. The resulting centrifuged mixture yielded a supernatant and a bacterial pellet. The supernatant, which contained liquid and other cellular debris, was carefully discarded. The bacterial pellet, which consists of concentrated bacterial cells, was retained and collected for further analysis or experimentation. For AgNP treatment experiments, bacterial cultures (1×10^7 CFU mL^{-1}) were inoculated into the amended Basal Medium (BM: 0.4 g L^{-1} yeast extract, 1 g L^{-1} peptone, 1 g L^{-1} sodium chloride) and on Basal Medium Agar (BMA: BM: 0.4 g L^{-1} yeast extract, 1 g L^{-1} peptone, 1 g L^{-1} sodium chloride and agar 15 g L^{-1}) at a 1% inoculum rate. A control group was included for each bacterial strain, where no AgNPs were introduced. To account for the potential influence of incident light reflectance by nanoparticles (NPs), negative controls consisting solely of AgNPs were included during the exposures. The absorbance values of these negative controls were then utilized to subtract any fluctuations observed in the inoculated cultures. All treatments were replicated at least three times,

Susceptibility of Bacterial Strains to Ag Nanoparticles

Strains of *G. vulcani* 2Cx, *B. licheniformis* 3CA, *P. macerans* 3CA1, *A. ayderensis* FMB1, and *B. paralicheniformis* FMB2-1 were cultivated in BM at 50 °C, pH 7.0 at optimal conditions.

In order to determine the AgNPs sensitivities/resistances of these bacterial strains, each strain was grown separately in liquid BM under optimum growth conditions and a

12-hour overnight culture was obtained. BM medium and various concentrations (62.5, 125, 250, 500, 1000 and 1500 µg mL^{-1}) of AgNPs were added to 15 mL sterile tubes and inoculated with equal amount of bacteria (0.1 mL) from the 12-hour fresh culture and incubated at 50 °C for 24 hours in an shaking incubator (at 100 rpm). AgNPs in different concentrations in which bacteria were not added was used as negative control, and the medium in which bacteria grown without AgNPs was used as positive control. At the end of the incubation, all samples tested for growth inhibition of bacterial cells by AgNPs were measured at 600 nm in the spectrophotometer (Libra Biochrom) and the absorbance values were obtained. The minimum inhibitory concentration (MIC) was determined as the lowest concentration of AgNPs that effectively inhibited bacterial growth by 99%. Cell viability was quantified by counting the number of colony-forming units (CFUs) per milliliter, and the calculation was performed using the following formula:

$$CFU\ mL-1 = \frac{(number\ of\ colonies\ x\ dilution\ factor)}{volume\ covered\ (mL)}$$

Uniformly spread from 0.1 mL of bacterial cultures into semi-solid BM agar medium and incubated as mentioned above. The MBC, representing the lowest AgNPs concentration at which all bacterial cells were completely eliminated in the medium, was determined.

Exploring Cellular Damage through Transmission Electron Microscopy (TEM)

All bacterial strains, with the exception of the control group, were exposed to the prepared AgNPs concentrations specified by 62.5, 125, 250 or 500 µg mL^{-1}. The bacterial cultures were exposed to the AgNPs and allowed to incubate under favorable growth conditions for 24 hours. After the incubation period, the bacterial cultures were subjected to centrifugation at room temperature at a speed of 10000 rpm for 10 minutes. The supernatant, which contained liquid and other cellular debris, was

carefully discarded and repeated the centrifuge cycle several times by adding sterile phosphate buffered saline (PBS 1x) with a concentration of 10 mM and a pH of 7.2. The cellular damage caused by AgNPs was observed using a Jeol brand (model JEM-1010) Transmission Electron Microscope (TEM), equipped with a GATAN brand 782 ES500W camera system. The speed voltage was increased to 120 kV to facilitate the observation process. To prepare the specimens for TEM analysis, a small amount of each cell suspension was carefully placed drop by drop onto copper grids. Subsequently, the grids were left to dry naturally at room temperature for a few hours. Once dried, the prepared specimens were ready for TEM imaging.

FT-IR Analysis of Bacterial Biomass Treated with Nanoparticles

Fourier transform infrared spectroscopy (FT-IR) analysis is conducted to qualitatively assess the surface functional groups of the materials. For this, all bacterial strains were grown overnight in BM medium at 50 °C. Following washing and centrifugation, each strain sample was supplemented with a final concentration of 500 µg mL^{-1} of AgNPs, while ensuring a cell density of 10^{8-9} CFU mL^{-1} was maintained. After incubating for 24 hours, the bacterial cultures, both treated with AgNPs and untreated, were subjected to centrifugation to separate the pellet. The resulting biomass was then dried at 60 °C under vacuum conditions in a vacuum incubator until it reached a weight of 2.5 mg. The biomass samples obtained were recorded in the FT-IR spectrophotometer device (Perkin Elmer Spectrum 100) in the reduced total reflection (ATR) system with a resolution of 16 cm-1 and a wavenumber range of 4000 to 450 cm^{-1} subjected to 20 scans.

Evaluating Cellular Viability in the Presence of NP Stress

All bacterial strains, except the control group, were subjected to treatment with the prepared AgNPs (62.5, 125, 250 or 500 µg mL^{-1}). The bacterial cultures were exposed

to the AgNPs and allowed to incubate under favorable growth conditions for 12 hours. After the incubation period, the bacterial cultures were assessed for cell viability.

Cell viability was evaluated using the MTT assay. PBS with a concentration of 10 mM and a pH of 7.2 was used as solvent to prepare a stock solution of 5 mg mL^{-1} of MTT 3-(4,5-Dimethyl-2-thiazolyl)-2,5-diphenyl-2H-tetrazolium bromide). The solution was then sterilized through filtration and were carefully maintained and stored at a precise temperature of -20°C for future applications. For each treatment, including the control, a volume of 500 µL of the cell suspension was carefully transferred to individual 1.5 mL microcentrifuge tubes. Subsequently, 50 µL of the MTT solution was integrated in each tube, and proper mixing was ensured by vortexing. The tubes were then placed in water bath shaker at a temperature of 50 °C and allowed to incubate for a duration of 1 hour. After the incubation period, the bacterial cultures underwent centrifugation at room temperature at a speed of 12000 rpm for 10 minutes to collect the pellet. The supernatant was thrown away, and 500 µL of 100% dimethyl sulfoxide (DMSO) was added to each tube. The tubes were incubated again at 30 °C for 30 min to dissolve crystalised formazan. Subsequently, a volume of 200 µL of the supernatant, which exhibited a distinctive purple colour, was carefully transferred to individual wells of a 96-well plate. Every single treatment was replicated twice, and blanks (PBS only) were included as negative controls for each group. The optical density of the samples was determined using a microplate reader (Multi ScanGo, Thermo) at 570 nm wavelength. The cell viability percentage was ascertained by employing the provided formula, which relies on absorbance values:

$$\% \text{ viability} = \frac{Absorbance\ of\ treated\ cells}{Absorbance\ of\ untreated/control\ cells} \ \%100$$

Quantifying Superoxide Generation in Bacterial Cells under NP-induced Stress

The bacterial cultures were exposed to the AgNPs to assess the generation of superoxide anions, as described in evaluating cellular viability in the presence of NP stress part. To prepare a stock solution of nitroblue tetrazolium (NBT), 8 mg mL^{-1} of NBT powder was meticulously dissolved in sterile ultra-purified water. The solution was then stored in a refrigerator at 4°C for future use. For each treatment followed by 12 hour incubation, including the control group, a precise volume of 200 µL of the cell suspension was meticulously transferred to individual wells of a 96-well plate. Each treatment was replicated twice to ensure reliability, and blanks consisting of phosphate-buffered saline (PBS) alone were included as negative controls for each group. Subsequently, a precise volume of 20 µL of the NBT solution was carefully added to each well containing the cell suspension. The plate was then incubated at a temperature of 50 °C with continuous shaking for a duration of 2 hours. During this incubation period, SOR released by the cells reacted with NBT, forming blue-colored formazan deposits. After the incubation period, the absorbance of the cell suspensions was measured at a wavelength of 570 nm using a microplate reader (Multi ScanGo, Thermo). This measurement allowed for the quantification of the deposited formazan and served as an indicator of superoxide anion generation by the cells.

Effect of Silver NPs on Enzyme Biosynthesis

In order to determine the β-galactosidase biosynthesis by bacterial strains, the liquid BM containing 2% lactose was prepared by adding several AgNP concentrations (62.5, 125, 250 or 500 µg mL^{-1}) and inoculated with the bacterial strains for 24 hours in a shaking incubator at 50 °C, and to facilitate cell permeabilization, a 650 µL portion of the culture sample was combined with an equal volume of 0.1 M sodium phosphate buffer (pH 7.0), and subsequently, 0.01% sodium dodecyl sulfate (SDS) was added to the mixture (as described in 56, 57) and incubated at 50 °C for 10 minutes. Following that, a solution of 60 mM o-nitrophenyl-β-D-galactopyranoside (oNPG) was introduced

to the mixture and allowed to incubate at 50 °C for an additional 10 minutes. The reaction was subsequently terminated by the addition of Na_2CO_3. Enzyme activity was measured in a spectrophotometer (Libra Biochrom) at 405 nm. The residual activity in the absence of AgNPs for all strains (controls) was taken as 100%. All data were the mean values of at least 3 experiments.

Effect of Silver NPs on Enzyme Secretion and Inhibition

Bacterial cultures were grown in BM broth supplemented with 2% lactose. When the bacterial cells reached the early exponential growth phase, they were separated by centrifugation at 10000 rpm for 10 minutes. The resulting pellets were resuspended in a solution of 0.02 M sodium phosphate buffer (pH 7.5) containing 0.01 M NaCl. Cell density was maintained at approximately 108-9 CFU mL^{-1}. For each strain, 500 µL of cell suspension was treated with 250 µg mL^{-1} AgNPs, along with non-treated controls containing only bacterial strains. The mixture was incubated for 4 hours at 50 °C in a shaking incubator (100 rpm). After the completion of the incubation period, 500 µL of a 0.02 M sodium phosphate buffer (pH 7.5) containing 0.01 M NaCl was added to both the control and treated cell suspensions. The supernatants obtained by centrifuging the suspensions at 12000 rpm for 10 minutes were used to assess the extracellular ß-galactosidase activity. The activity was measured at 405 nm using oNPG as the substrate on a spectrophotometer. All data were the mean values of at least 3 experiments.

Bacterial strains namely *A. ayderensis* FMB1 and *B. licheniformis* 3CA which extracellularly secrete the enzyme more efficiently compared to others were also utilised in order to determine whether various AgNP concentrations inhibit the activity of β-galactosidases. The cultures were produced under optimum conditions in AgNP-free liquid BM and supernatants were obtained by centrifugation. Then, 500 µL 0.02 M sodium phosphate buffer (pH 7.5) containing AgNPs (final concentrations between

62.5 to 250 µg mL^{-1}) was added to 500 µL of each supernatant and incubated at 50 °C for 30 min for the interaction of nanoparticule and enzyme. At the end of this period, and the reaction was carried out by adding oNPG and incubated at 50 °C for 10 min. The enzyme activity was measured spectrophotometrically at 405 nm. The crude enzyme samples without added AgNPs were used as control (the relative activities were considered as 100%) and the relative activities were determined by calculating the average of at least three replicates.

Statistical Analysis

The data obtained from the experiment underwent statistical analysis utilizing one-way analysis of variance (ANOVA) with a significance level set at 5%. The least significant difference (LSD) was computed as a measure to assess the variation between the means of different treatments. In addition, for comparing the differences among the treatment means, Duncan's multiple range test (DMRT) was utilized at a significance level of 5%. The data depicted in the figures were represented as the mean ± standard deviation (SD) and were based on two independent replicates conducted for each measured parameter.

Results and Discussion

Determination of Silver (Ag) Ion Release from AgNPs

To explore the extent of ionic silver dissolution from AgNP, which may cause cellular toxicity, AgNPs at 250 µg mL^{-1} was evaluated after 24 hours incubation. The calculated dissolved silver (Ag) was found to be as low as 0.55 % in basal medium at 50 $^{\circ}$C.

The inclusion of silver nanoparticles in a wide range of manufactured goods contributes to their discharge into aquatic ecosystem, leading to the presence of dissolved silver

(Ag+) and subsequently exerting toxic impacts on diverse aquatic life forms, including bacteria, algae, fish, and daphnia [58]. NPs can easily enter the cellular entities through inhalation, ingestion, or skin absorption due to their nano-scale size. This property allows them to have significant interactions within the human and other living organisms [59]. There have been ongoing debate that Ag+ released from AgNPs was the main factor in cellular toxicity as it readily enters the cells, inhibiting several vital functions [24]. Metal ions slowly released from NP interact with the functional groups of biomolecules, inhibiting of enzyme activities, altering the cell structure, interfering with the normal physio-logical processes, and finally affecting the microorganism [26]. On the other hand, the toxic effects of AgNPs may probably be due to AgNP itself binding to biomolecules leading to inhibition of protein biosynthesis and enzyme activity [27,34].

The bactericidal actions of silver ion itself determined by MICs and MBCs against various pathogens were investigated and the MICs and MBCs of silver ion were found to range from 1.9-15.6 µg/ml [60]. Moreover, the MICs and MBCs of ionic silver and chemically produced nanosilver were compared in growth medium for three bacterial species namely *E. coli, P. aeruginosa,* and *S. aureus* after 24 h of exposure. For all three bacteria, the MIC and MBC values for nanosilver were 500 µg/mL or above, while it ranged between 12,5-200 µg/mL for ionic silver [61]. From this point of view, it seems antibacterial effects of silver ions to be seen at rather high concentrations, and thus extremely low Ag$^+$ release from AgNPs (0.55 %) could not be considered as the only cause of toxicity on the thermophilic bacteria. Zhang et al. [62] also found that the amount of Ag+ released from AgNPs were less than 0.5% and discussed that the partial reduction in toxicity for mesophilic bacteria may be attributed to a decrease in release of silver ions.

Phenotypic Characterization of Bacterial Strains

The strains of *G. vulcani* 2Cx, *B. licheniformis* 3CA, *P. macerans* 3CA1, *A. ayderensis* FMB1, and *B. paralicheniformis* FMB2-1 were Gram-positive and rod-shaped. Bacterial strains having varying morphological and physiological features are shown in Table 2.

Table 2. Morphological and physiological features of the strains

Bacterial strains	Shape	Spore forming	Pigmentation	Optimum temperature (°C)	Optimum pH	Reference
G. vulcani 2Cx	rod	+	light yellow	55	7.0	[53]
B. licheniformis 3CA	rod	+	creamy white	55	8.0	[53]
P. macerans 3CA1	rod	+	creamy white	50	7.0	[53]
A. ayderensis FMB1	rod	+	yellow/orange	50	7.0	[54]
B. paralicheniformis FMB2-1	rod	+	creamy white	50	7.0	[55]

Bacterial Growth and NP Tolerance/Sensitivity

The strains of *G. vulcani* 2Cx, *B. licheniformis* 3CA, *P. macerans* 3CA1, *A. ayderensis* FMB1, and *B. paralicheniformis* FMB2-1 grown in a specific basal medium exposed to various AgNP concentrations (62.5−1500 µg mL^{-1}) showed differential resistance/sensitivity behavior. MIC and MBC of AgNPs against *G. vulcani* 2Cx, *B. licheniformis* 3CA, *P. macerans* 3CA1, *A. ayderensis* FMB1, and *B. paralicheniformis* FMB2-1 are shown in Table 3.

Table 3. MIC and MBC of AgNPs against thermophilic bacteria

Bacterial strains	AgNPs (µg mL−1)	
	MIC	MBC
G. vulcani 2Cx	500	1000
B. licheniformis 3CA	1000	1500
P. macerans 3CA1	500	1000
A. ayderensis FMB1	1000	1500
B. paralicheniformis FMB2-1	500	1000

In Table 3, the MIC (minimum inhibitory concentration) and MBC (minimum bactericidal concentration) values of AgNPs against five different strains of thermophilic bacteria are presented. The highest concentration of AgNPs (1000 or 1500 µg mL^{-1}) was found to be ineffective in determining the MIC and MBC values against certain strains of thermophilic bacteria. The results demonstrated a significant reduction in cell numbers at lowest levels at the corresponding MIC, and a complete lost was observed at the MBC. Figure 1 shows the growth inhibition of thermophilic bacteria strains depending on the increasing concentrations of AgNPs. It is evident that the strains *G. vulcani* 2Cx and *B. paralicheniformis* FMB2-1 exhibit higher sensitivity to AgNP treatments. There was a sharp growth inhibition (71.1%) for *G. vulcani* 2Cx in the presence of AgNPs even at 62.5 µg mL^{-1} compared to the control, while the growth was decreased slowly between 62.5 -1000 µg mL^{-1} AgNP concentrations. Moreover, *B. paralicheniformis* FMB2-1 growth also appears to be inhibited sharply between 62.5 µg mL^{-1} to 500 µg mL^{-1} AgNP concentrations. In contrast, the growth inhibition of *P. macerans* 3CA1 is minimal at AgNP concentrations of 62.5 and 125 µg mL^{-1}, with only 2.6% and 15.6% inhibition, respectively. However, a pronounced inhibition of 72.5% is observed at the concentration of 250 µg mL^{-1}. However, it can also be seen that growth inhibition for

A. ayderensis FMB1 and *B. licheniformis* 3CA are decreased consistently at AgNP concentrations starting from 62.5 upto 1000 µg mL^{-1}.
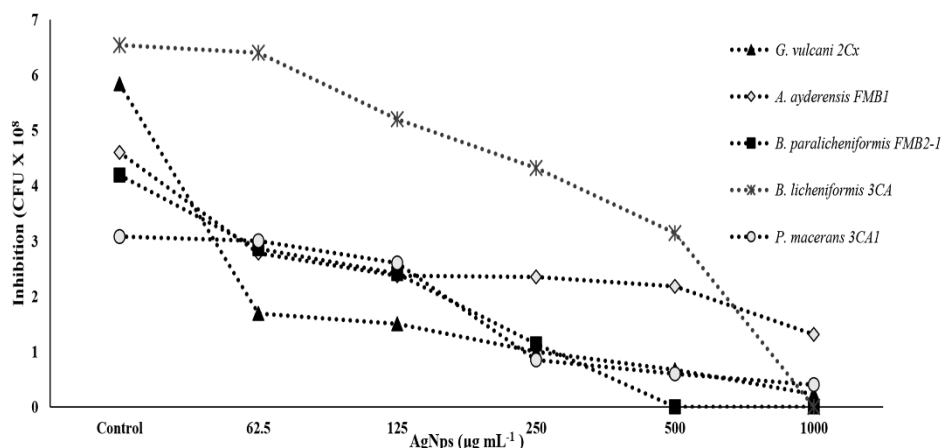

Figure 1: Concentration-dependent growth inhibition of bacterial cells by AgNPs. All samples were measured at 600 nm in the spectrophotometer and the absorbance values were converted to colony forming units.

The antibacterial effect of AgNPs is attributed to their small particle size, which allows for excellent penetration into bacteria, especially Gram-negative bacteria. Furthermore, this effect is known to be concentration-dependent, meaning that higher concentrations of AgNPs result in increased antibacterial activity [14,15]. The growth inhibition for *S. aureus* was found to be less remarkable (MIC value of 33 nM), while even low AgNPs concentrations inhibited *E. coli* growth (MIC of 3.3 nM) considerably [11]. Ahmed et al., [63] also studied the impact of metal NPs on the growth behavior of soil bacteria such as *S. meliloti*, *P. mosselii*, *A. chroococcum* and *B. thuringiensis* revealed that all sub-MIC concentrations of metal NPs delayed the bacterial growth for all test strains, while higher concentrations abolished the growth totally. In case of AgNPs, the MIC concentrations were observed as 1000, 500, 250 and 500 µg mL^{-1},

19

while the MBC concentrations were 1500, 1000, 500 and 1000 µg mL^{-1} for *B. thuringiensis*, *P. mosselii,* S*. meliloti* and *A. chroococcum,* respectively.

Exploring Cellular Damage through Transmission Electron Microscopy (TEM)

The observed effects of AgNPs on thermophilic bacterial strains, as visualized through transmission electron microscopy (TEM), varied in terms of their destructive potential (Figure 2A-J). The images showed that the thermophilic strains grown in the absence of AgNPs mostly had undamaged and intact structures, while AgNP treated cells were broken and destructed with many fragmented cell envelopes. The leakage of cytoplasmic content from inside the cells was observed in certain species, notably in *G. vulcani* 2Cx and *P. macerans* 3CA1, providing clear evidence of cellular damage (Figure 2B and J).
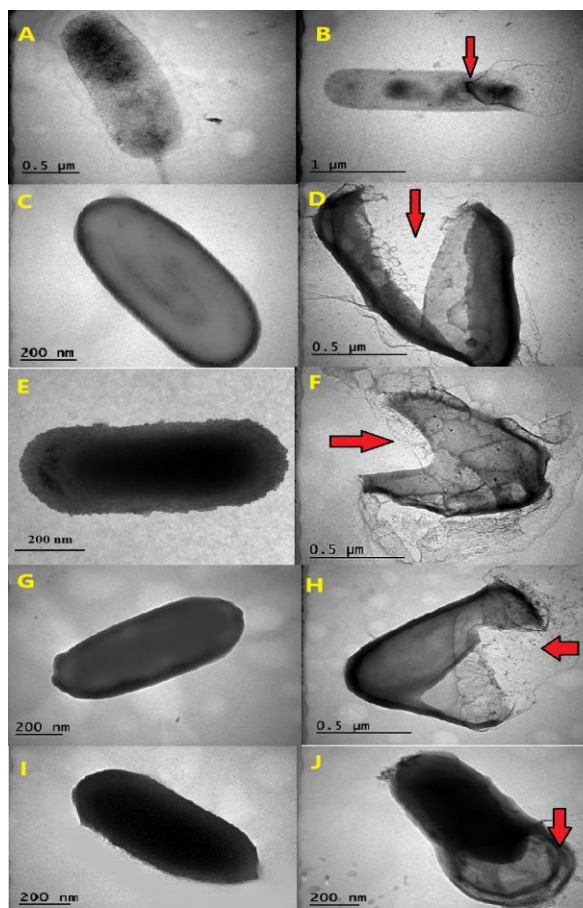
Figure 2. The effects AgNPs on the morphology of thermophilic bacteria. TEM images of untreated cells of *G. vulcani* 2Cx (A), *A. ayderensis* FMB1(C), *B. paralicheniformis* FMB2-1 (E), *B. licheniformis* 3CA (G) and *P. macerans* 3CA1(I), and after exposure of each strains to various AgNP concentrations (B, D, F, H, J). Red arrows indicate cellular damage.

The transmission electron micrographs of AgNP-treated and untreated biomass of all thermophilic bacterial strains clearly show that AgNPs interact with bacterial cells and thus had severe inhibitory effects which caused structural damage in cell walls of thermophilic bacteria (Figure 2A-J).

TEM analysis conducted in a previous study has provided evidence that the exposure of E. coli cells to AgNPs results in rapid and complete disruption of the cell membrane within a few minutes. The interaction between AgNPs and the thiol groups of proteins

in the cell wall causes irreversible structural changes, resulting in the disruption of the cell wall and the formation of multiple pits at the sites affected by AgNPs [64].
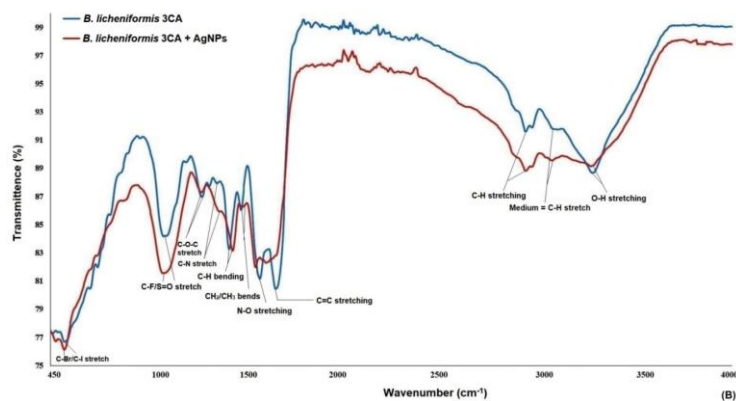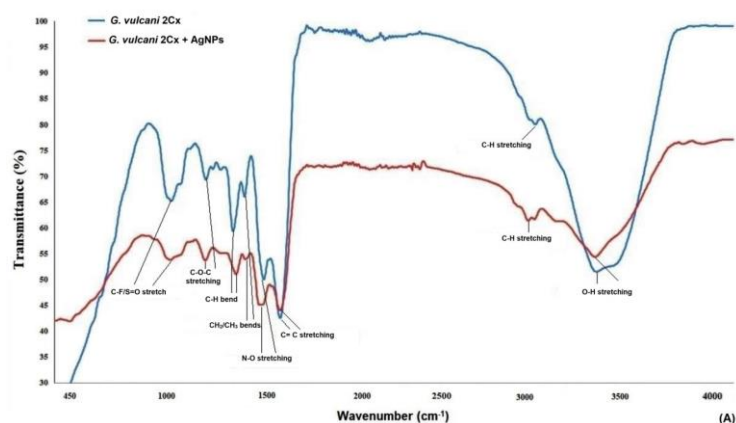
Analysis of AgNP-Treated Bacterial Biomass Using FT-IR

Figure 3 A-C illustrates the FT-IR (Fourier transform infrared spectroscopy) data of AgNPs obtained from the selected three strains, *G. vulcani* 2Cx, *B. licheniformis* 3CA, and *A. ayderensis* FMB1. Significant changes were observed in the spectra, specifically in the peaks corresponding to different functional groups present on the surface of bacterial cells. Significant changes were observed in the FT-IR spectrum of the AgNP-treated bacterial cell biomass, with notable alterations characterized by the narrowing and shifting of peaks. In average, the presence of carbon-related component, lipids, DNA, and proteins, amino-related component, polysaccharides and other aromatic organic compounds as most frequent biomolecules were indicated by the IR signals in both control and AgNP-treated samples for all bacterial strains [65-68].

FT-IR analysis has been used previously for evaluating significant variations of various functional groups present on the cell surface of bacteria after treating with different nanoparticles. For instance, silver and zinc nanoparticles were discovered to induce slight modifications in functional groups of soil bacteria such as *Azotobacter chroococcum* and *Pseudomonas mosselii*, as compared to the control group. This observation suggests that the inhibitory effects of nanoparticles on bacterial cells may lead to structural damage especially cell membrane, thereby causing disruptions in the biochemical composition of the cells [63]. In a separate investigation, FT-IR was employed to elucidate the binding of fullerenol, a carbon nanostructure measuring 1 nm, to the lipid bilayer structure of a model bacterial cell. The analysis revealed that

the OH groups present in the lipid layers were identified as the most active functional group during this binding process [69].

The analysis of the xenobiotic interactions with biomolecule functional groups of cells by FT-IR is well documented for α-helix protein (with spectral band displayed at 1655-1658 cm^{-1}), membrane lipids (at 2854 cm^{-1} and 2924 cm^{-1}) and nucleic acids (at 1124 cm^{-1} ve 1082 cm^{-1}) [70-73]. The results obtained from FT-IR spectra in the present study revealed notable changes observed by the narrowing and shifting of peaks indicating the interactions of AgNPs with the cell walls, protein and enzymes, and DNA in thermophilic bacteria. These are in aggrement with our results obtained also with MIC, MBD, TEM images, generation of ROS and inhibition of enzyme biosynthesis and secretion.
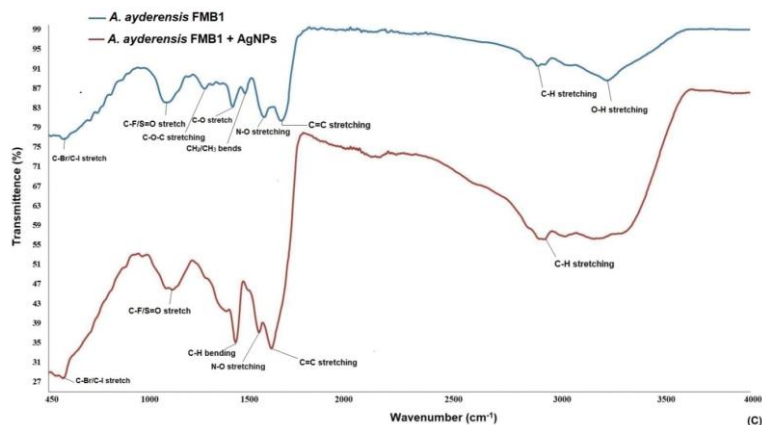

23

Figure 3. FT-IR (Fourier transform infrared spectroscopy) data of both AgNP-treated (500 µg mL⁻¹) and untreated bacterial biomasses from *G. vulcani* 2Cx, *B. licheniformis* 3CA, and *A. ayderensis* FMB1 exposed to 24-hour incubation.

Evaluating Cellular Viability in the Presence of AgNP Stress

The MTT assay finds extensive applications in the field of microbiology, primarily for the spectrophotometric evaluation of the metabolic activity exhibited by microorganisms [74]. Confirmation of cellular metabolism related to dehydrogenase activity was achieved by the formation of a distinct purple color, with the control group displaying the highest cellular activity and exhibiting the darkest coloration. The metabolic activity loss of bacterial cells is represented by a decrease in colour intensity shown in microtiter wells (Figure 4A). The metabolic activity of all five bacterial strains, as indicated by the cell viability percentage (%), demonstrated a substantial reduction with increasing concentrations of AgNPs, i.e., ranging from 62.5 µg mL^{-1} to 1000 µg mL^{-1} (Figure 4 B-F). At a concentration of 62.5 µg mL^{-1} of AgNPs, *G. vulcani* 2Cx exhibited the lowest cell viability, with a recorded value of 61.87% (Figure 4B). In contrast, *B. licheniformis* 3CA demonstrated the highest cell viability at this concentration, with a remarkable value of 83.96% (Figure 4C). Furthermore, at 125 µg mL^{-1} concentration, *G. vulcani* 2Cx showed lowest viability (27.07%) (Figure 4 B), however, no noteworthy variations were observed among the rest of the bacterial

24

strains at this concentration (Figure 4 C-F). At 250 µg mL^{-1} on the other hand, the lowest viability (25.75%) was observed in *G. vulcani* 2Cx whereas the highest cell viability (39.02%) was found in *B. paralicheniformis* FMB2-1 bacterial strain ((Figure 4 B & F). At the highest AgNPs concentration (1000 µg mL^{-1}), *P. macerans* 3CA1 exhibited the lowest cell viability by 17.86 % (Figure 4D).
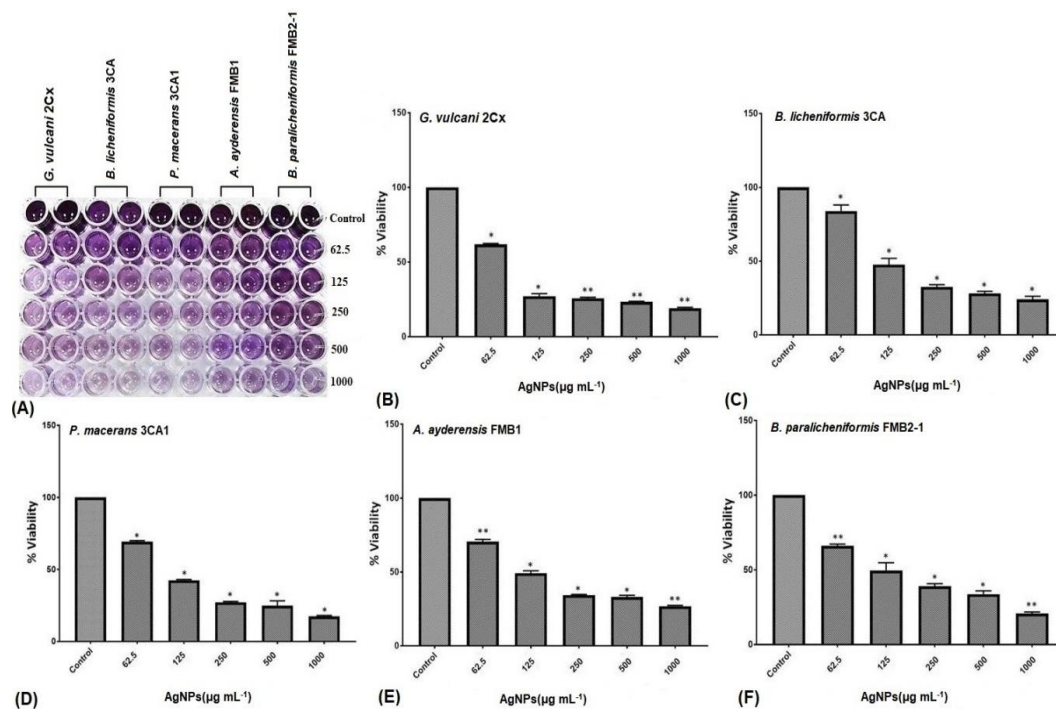

Figure 4. Inhibition of cellular viability of *G. vulcani* 2Cx (B), *B. licheniformis* 3CA (C), *P. macerans* 3CA1 (D), *A. ayderensis* FMB1 (E), *B. paralicheniformis* FMB2-1 (F) exposed to the AgNPs concentrations of 62.5−1000 µg mL^{-1} including control. (A) The diminishing intensity of the purple color observed in the 96 wells plates indicates a decrease in the metabolic activity of the bacterial cells. Asterisks represent significant difference at at *P ≤ 0.02 and **P ≤ 0.0076.

Supporting results were also obtained from a previous study that utilized the TTC assay to evaluate the cell viability of several soil bacteria, including *B. thuringiensis, P. mosselii, S. meliloti,* and *A. chroococcum*, under the influence of silver and zinc oxide

nanoparticles (62.5−1000 µg mL^{-1}). The study assessed cellular respiration, particularly dehydrogenase activity, and the results indicated a significant decrease in cellular respiration when bacteria were exposed to the highest concentration of both AgNPs and ZnONPs [63].

Quantifying Superoxide Generation in Bacterial Cells under AgNP-induced Stress

Under the influence of 62.5−1000 µg mL^{-1} AgNPs, all five bacterial strains exhibited the production of the superoxide radicals (SOR; O$_2^-$), which subsequently facilitated the reduction of nitro blue tetrazolium (NBT) to formazan. The resulting formazan formation was quantified using spectrophotometric methods (Figure 5 A). *G. vulcani* 2Cx exhibited the maximum production of SOR radicals at AgNPs concentrations of 125 and 250 µg mL^{-1} by the absorbance rate of 2.01 and 2.04 correspondingly (Figure 5B).

For control and AgNPs concentration of 62.5 µg mL^{-1} maximum SOR production was observed in *P. macerans* 3CA1 with significant absorbance of 1.50 and 1.78, respectively (Figure 5B). On the other hand, *A. ayderensis* FMB1 demonstrated the highest production of SOR radicals at AgNPs concentrations of 500 and 1000 µg mL^{-1} with the corresponded absorbance of 2.23 and 2.26, while the lowest production was obtained in the untreated control group (1.17) (Figure 5B).
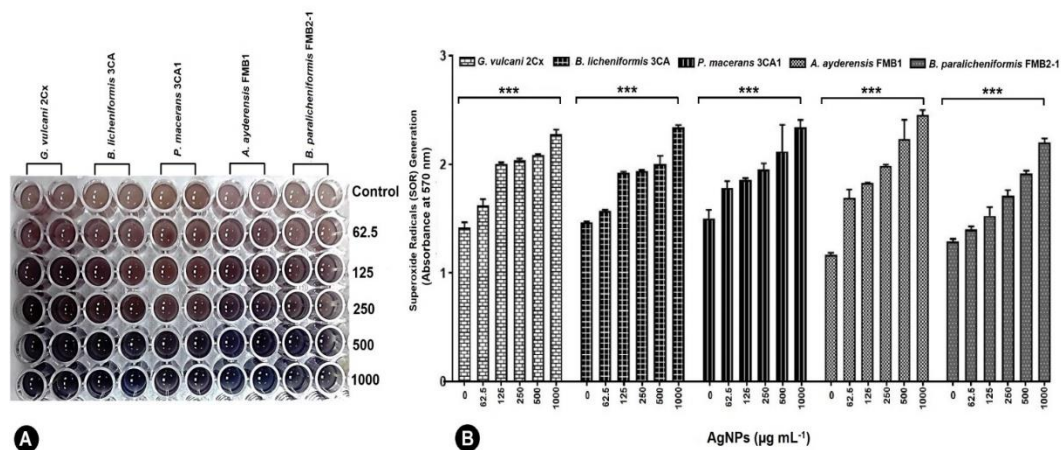
Figure 5. Generation of superoxide radicals (SOR) by *G. vulcani* 2Cx, *B. licheniformis* 3CA, *P. macerans* 3CA1, *A. ayderensis* FMB1, and *B. paralicheniformis* FMB2-1 exposed to the AgNPs concentrations of 62.5−1000 µg mL^{-1} including control (B). (A) The presence of a blue-colored formazan, developed intracellularly in the 96-well plates, signifies an augmented production of SOR. Asterisks indicate significant difference at ***$P \leq 0.0004$.

Reactive oxygen species (ROS) occur due to incomplete oxygen reduction within different metabolic pathways, serving as by-products in these processes. Their presence at low concentration is indispensable for maintaining cellular functionality, and their concentration within the cellular system is intricately regulated by the intricate antioxidant defense system [75]. Ensuring that intracellular ROS production remaining within the physiological range is advantageous for cellular health and functioning. However, elevated levels of intracellular ROS can trigger apoptosis, a process of programmed cell death [76].

Moreover, exposure of silver NPs to human cells induces genotoxicity, cytotoxicity, and inflammation in a cell-type dependent manner. Oxidative stress-dependent toxicity of AgNPs has been also well documented in animals [77,78]. Ahmed et al., [63] found that SOR production increased with an increasing concentration of metal NPs in

beneficial soil bacteria. Elevation of cellular oxidative stress in microorganisms has been an important antibacterial mechanism of metallic NPs and heavy metals ions, such as Ag (+). The generation of reactive oxygen species (ROS) and and free radical species is responsible for the potent antiviral, antifungal, and antibacterial activity exhibited by AgNPs. The ROS includes hydrogen peroxide (H_2O_2), singlet oxygen (O_2), superoxide radical (O_2^-), hydroxyl radical ($OH^{\cdot}$), and hypochlorous acid ($HOCl$). AgNPs treatment of bacterial cells leads to ROS production and subsequent oxidative stress, which induces cell death, possibly through the hyperoxidation of proteins, lipids, and DNA [79,80].

Effect of Silver NPs on Enzyme Biosynthesis

In order to determine the inhibition of β-galactosidase biosynthesis in bacterial cells, only four thermophilic bacteria strains in the presence of sub-MIC concentrations of AgNPs between 62.5 to 500 µg mL^{-1} were grown in liquid BM for 24 hours in a shaking incubator at 50 °C. *P. macerans* 3CA1 was excluded here because the growth was not consistent throughout the experiment. Figure 6 shows both the inhibition of bacterial growth and β-galactosidase biosynthesis in tested thermophilic bacteria exposed to specified AgNP concentrations in the same experiments set. After a 24-hour exposure, the β-galactosidase activity of *G. vulcani* 2Cx decreased to 41% at 62.5 µg mL^{-1} AgNP and further decreased to 28.8% at 500 µg mL^{-1}, compared to the untreated controls with 100% relative activity. Likewise, for *A. ayderensis* FMB1, the activity decreased to 45.9% at 62.5 µg mL^{-1} AgNPs and 32.2% at 250 µg mL^{-1} whereas for *B. licheniformis* 3CA, the activity decreased to 38.8% at 62.5 µg mL^{-1} AgNPs, potentially reaching complete inhibition. In addition, for *B. paralicheniformis* FMB2-1, it was observed that the activity was not affected much by 91.2% in the presence of 62.5 µg mL^{-1} AgNPs, but decreased sharply to 11.2% at AgNPs concentration of 125 µg mL^{-1} (Figure 6).
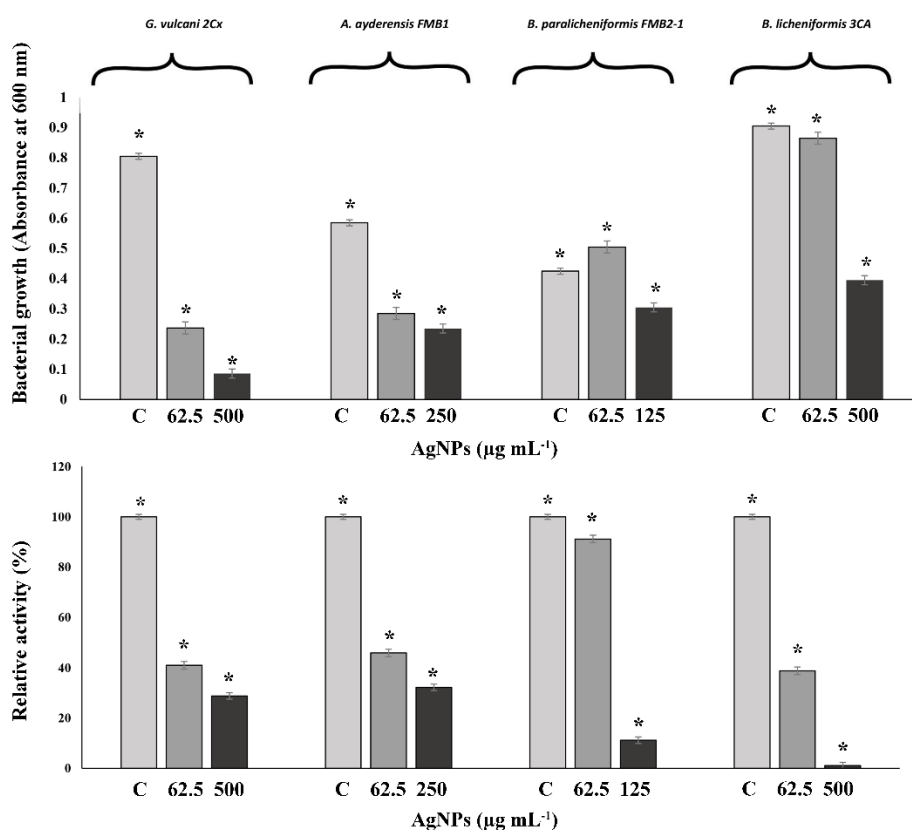
Figure 6. The effects of AgNPs on bacterial growth and levels of β-galactosidase biosynthesis in tested thermophilic bacteria. Upper chart shows bacterial growth inhibition of *G. vulcani* 2Cx, *A. ayderensis* FMB1, *B. paralicheniformis* FMB2-1 and *B. licheniformis* 3CA exposed to specified AgNP concentrations of 62.5, 125, 250 or 500 µg mL^{-1}. Lower chart indicates inhibition of β-galactosidase biosynthesis expressed by these strains exposed to the same concentrations of AgNPs during 24 h incubation. Absorbance of *o*-nitrophenol (yellow coloured-end product of the substrate ONPG) measured at 405 nm obtained for controls (taken as 100% relative activity) is plotted against absorbances obtained for treated samples. Values are mean of three independent experiments ± SD. Asterisks indicates significant difference at *$P < 0.001$.

β-Galactosidase also known as a glycoside hydrolase enzyme hydrolyzes galactopyranosides such as lactose, and produces galactooligosaccharides by

29

catalyzing the trans-galactosylation reaction. Recent studies have focused on thermostable β-galactosidases obtained from thermophiles. There are studies on beta-galactosidase obtained from thermophilic bacteria such as *Alicyclobacillus acidocaldarius* subsp. rittmannii [47,48], *Bacillus licheniformis* KG9 [49], *Anoxybacillus* sp. KP1 [50], *A. ayderensis* [81], *Anoxybacillus* sp. FMB1 [82], *Anoxybacillus* sp. AH1 [83], *B. subtilis* 4NK and *B. paralicheniformis* 5NK [51]. Thermophilic *β*-galactosidases are used in many biotechnological fields such as in medical settings to address lactose intolerance, in the food industry to prevent crystallization of lactose in dairy products, and in environmental contexts to mitigate water pollution stemming from whey.

Notably, sodium dodecyl sulfate (SDS) has been employed as a membrane permeabilizer to facilitate the uptake of *o*NPG, a substrate typically impermeable to the cytoplasmic membrane, into bacterial cells, which is crucial for accurately quantifying the β-galactosidase activities exhibited by the tested bacterial strains. SDS plays a vital role in enhancing the penetration of *o*NPG into the cytoplasm, enabling the reliable measurement of β-galactosidase enzyme activity. In a previous study, we demonstrated that heavy metals alone significantly inhibited the biosynthesis of α-amylase and β-galactosidase in both *E. coli* and *B. subtilis* [56].

Substantional inhibition of β-galactosidase biosynthesis and its extracellular secretion in the thermophilic bacteria (please see Figures 6 and 7) may results from AgNPs enterance to the bacterial cell, binding to cellular structures and biomolecules such as DNA, lipids and proteins, and thus causing lethal toxic effects to microorganisms. Particularly, the interaction of AgNPs with ribosomes induces their denaturation, leading to the inhibition of translation and protein synthesis. This disruption of ribosomal function hinders the crucial processes involved in protein production, causing a notable reduction in protein synthesis [14,84,85]. AgNPs was also found to bind and inactivate cytoplasmic proteins needed for production of ATP, and thus

disrupting cellular functions. Additionally, AgNPs interact with disulfide bonds and block the active sites, resulting in the inactivation of enzymes and proteins that are associated with the cell membrane [86]. It is also shown that AgNPs have been observed to interact with the carboxyl and thiol groups of β-galactosidase, resulting in the inhibition of critical intracellular processes and ultimately culminating in cell death [87]. Protein synthesis has also been inhibited by Ag ions by preventing tRNA binding with ribosome subunit [88]. Ionic silver (Ag+) is known for its affinity to interact with -SH groups found in proteins and enzymes, resulting in conformational changes in their tertiary structure. This interaction disrupts the proper binding of substrates to their respective active sites, thereby affecting the functional activity of these biomolecules [89].

Effect of Silver NPs on Enzyme Secretion and Inhibition

In order to determine the inhibition effect of β-galactosidase secretion to outside of bacterial cells, bacteria grown in BM containing 2% lactose were treated with sub-MIC concentration of AgNPs (250 µg mL^{-1}) and the extracellular enzyme activities in supernatants were measured after 4 hours incubation. Samples without added AgNPs were used as controls. Figure 7A shows the effect of AgNPs on enzyme secretion by bacterial cells. It is seen that compared to the untreated controls (100 % relative activity), in the presence of 250 µg mL^{-1} AgNP, the enzyme secretion by thermophilic bacteria was reduced to 31.9% for *G. vulcani* 2Cx, 32.4% for *A. ayderensis* FMB1, 42.9 % for *B. paralicheniformis* FMB2-1, 3.3% for *B. licheniformis* 3CA and 9.7% for *P. macerans* 3CA1.
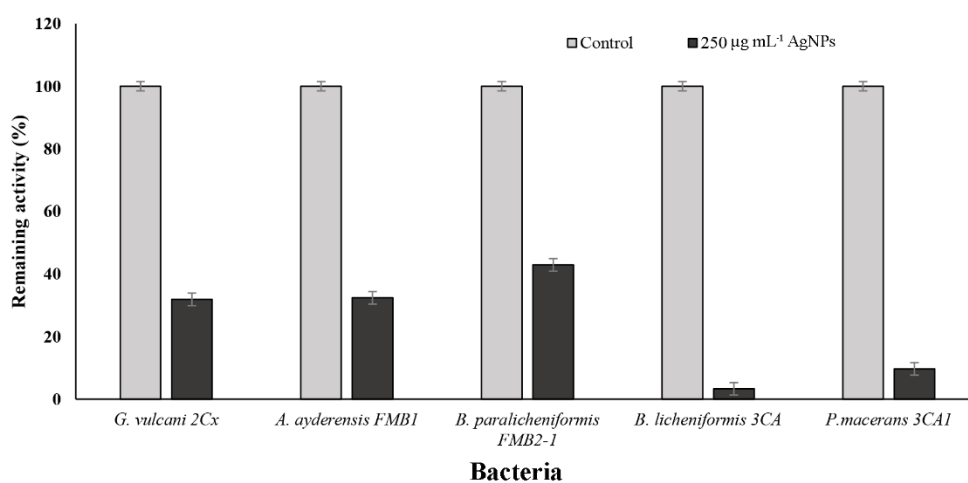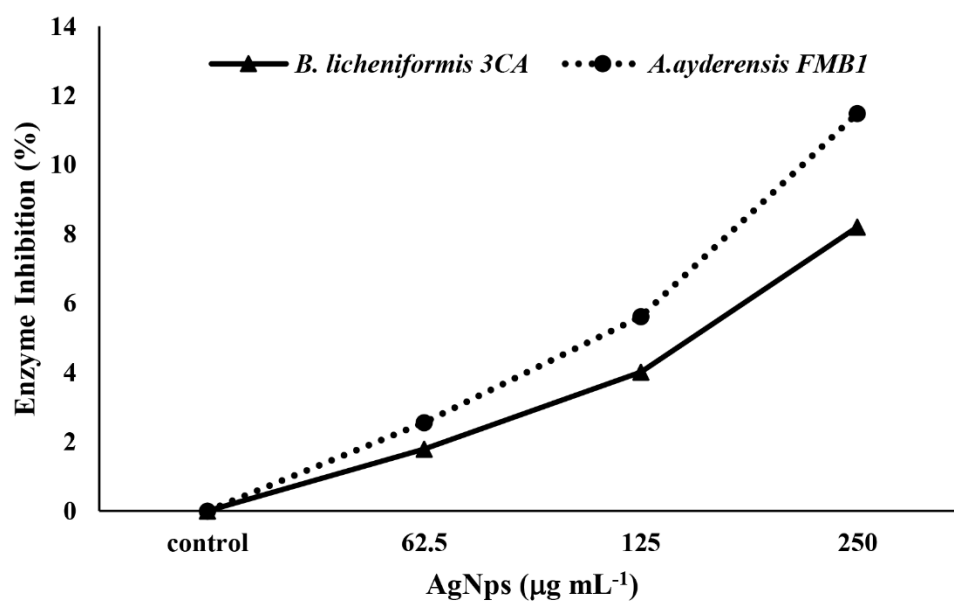
A

B

Figure 7. The effects of AgNPs on β-galactosidase secretion and crude enzyme inhibition. (A) Inhibition of enzyme secretion by bacterial strains *G. vulcani* 2Cx, *A. ayderensis* FMB1, *B. paralicheniformis* FMB2-1, *B. licheniformis* 3CA and *P. macerans* 3CA1. Each was exposed to a concentration of 250 μg mL^{-1}. (B) Inhibition of crude β-galactosidases of *A. ayderensis* FMB1 and *B. licheniformis* 3CA exposed to 62,5, 125 and 250 μg mL^{-1} sub-MIC AgNP concentrations. Absorbances of *o*-nitrophenol

measured at 405 nm obtained for controls (taken as 100% relative activity) are plotted against absorbances obtained for treated samples. Values are mean of three independent replicates ± SD.

In Figure 7B, the graph depicts the inhibition of extracellular enzymes in samples subjected to different sub-MIC concentrations of AgNPs. Comparatively, in comparison to the untreated control, inhibition of crude enzyme activity in all tested AgNP concentrations was not considerable, only 2.6% and 11.5% for the enzyme of *A. ayderensis* FMB1 in the presence of 62.5 µg mL^{-1} and 250 µg mL^{-1} AgNP, respectively, while it was 1.7% and 8.2% inhibition for that of *B. licheniformis* 3CA, respectively.

The exact mechanism underlying the antimicrobial effects of metal nanoparticles is still not fully comprehended. However, numerous studies have provided evidence for the lethal effect and growth inhibition of bacteria resulting from the destructive impact of AgNPs. These effects are attributed to the direct interaction between AgNPs and biomolecules on the bacterial surface through electrostatic attraction. This interaction leads to various consequences, including alterations in cell morphology, penetration of AgNPs into the cytoplasm alongside ions, increased membrane permeability due to membrane damage, cytoplasmic leakage, and the generation of intracellular oxidative stress in the form of superoxide anions. This oxidative stress progressively damages cellular constituents and membranes, disrupts the electron transport chain, halts the respiratory process, and causes the destruction of enzyme activity and denaturation of proteins. Ultimately, these combined effects result in the eventual death of the bacterial cells [90,91].

Conclusion

The present study puts emphasis on the toxic effects of AgNPs on the morphological, physiological and biochemiacal aspects including enzyme biosynthesis and secretion in thermophilic bacteria. Although five thermophilic strains exposed to AgNPs had a growth decrease in the number of CFU mL^{-1}, *G. vulcani* 2Cx and *B. paralicheniformis* FMB2-1 were more sensitive to AgNPs. AgNPs at all tested concentrations exhibited severe structural damage on thermophilic bacteria causing cytoplasmic leakage, broken and distructed cells. There were also a significant reduction in cell viabilities and enhanced superoxide radical (SOR) generation consistently with an increasing dose rate of AgNPs. Conclusively, AgNP treatments caused a significant inhibition of thermostable β-galactosidase biosynthesis and extracellular secretion by potent thermophilic strains likely to be used in various areas of industry. The mechanisms of the antimicrobial properties and toxicological effects of metallic NPs are not fully understood yet and need to be focused in the future work.

Author Contributions

Author Contributions: Conceptualization, K.G., F.M.B. and I.J.; methodology, K.G., F.M.B. and I.J.; validation, K.G., F.M.B. and I.J.; investigation, K.G., F.M.B, A.T and I.J.; resources, K.G. and I.J. ; data curation, F.M.B. and I.J.; writing—original draft preparation, K.G., F.M.B. and I.J.; writing—review and editing, K.G. All authors have read and agreed to the published version of the manuscript.

References

1. Nafisi, S.; Maibach, H. I. *Cosmet. Sci. Technol.* **2017**, 337–369. https://doi.org/10.1016/b978-0-12-802005-0.00022-7.
2. Keller, A. A.; Vosti, W.; Wang, H.; Lazareva, A. *J. Nanoparticle Res.* **2014**, *16* (7). https://doi.org/10.1007/s11051-014-2489-9.

3. Pourzahedi, L.; Vance, M.; Eckelman, M. J. *Environmental Science & Technology*, **2017**, 51(12), 7148–7158. https://doi.org/10.1021/acs.est.6b05923.

4. Vance, M. E.; Kuiken, T.; Vejerano, E. P.; McGinnis, S. P.; Hochella, M. F.; Rejeski, D.; Hull, M. S. *Beilstein J. Nanotechnol.* **2015**, *6,* 1769–1780. https://doi.org/10.3762/bjnano.6.181.

5. Laurent, S.; Forge, D.; Port, M.; Roch, A.; Robic, C.; Vander Elst, L.; Muller, R. N. *Chem. Rev.* **2010**, *110* (4), 2574–2574. https://doi.org/10.1021/cr900197g.

6. Sudha, P. N.; Sangeetha, K.; Vijayalakshmi, K.; Barhoum, A. *Emerging Applications of Nanoparticles and Architecture Nanostructures* **2018**, 341–384. https://doi.org/10.1016/b978-0-323-51254-1.00012-9.

7. Martis, E.; Badve, R.; Degwekar, M. *Chron. Young Sci.* **2012**, *3* (1), 68. https://doi.org/10.4103/2229-5186.94320.

8. Stampoulis, D.; Sinha, S. K.; White, J. C. *Environ. Sci. Technol.* **2009**, *43* (24), 9473–9479. https://doi.org/10.1021/es901695c.

9. Li, W.-R.; Xie, X.-B.; Shi, Q.-S.; Zeng, H.-Y.; OU-Yang, Y.-S.; Chen, Y.-B. *Appl. Microbiol. Biotechnol.* **2009**, *85* (4), 1115–1122. https://doi.org/10.1007/s00253-009-2159-5.

10. Zhang, X.-F.; Liu, Z.-G.; Shen, W.; Gurunathan, S. *Int. J. Mol. Sci.* **2016**, *17* (9), 1534. https://doi.org/10.3390/ijms17091534.

11. Tran, Q. H.; Nguyen, V. Q.; Le, A.-T. *Adv. Nat. Sci.: Nanosci. Nanotechnol.* **2013**, *4* (3), 033001. https://doi.org/10.1088/2043-6262/4/3/033001.

12. Nie, P.; Zhao, Y.; Xu, H. *Ecotoxicol. Environ. Saf.* **2023**, *253*, 114636. https://doi.org/10.1016/j.ecoenv.2023.114636.

13. Ramalingam, B.; Parandhaman, T.; Das, S.K. *ACS Appl Mater Interfaces.* **2016**, *8*(7), 4963–4976.

14. Morones, J. R.; Elechiguerra, J. L.; Camacho, A.; Holt, K.; Kouri, J. B.; Ramírez, J. T.; Yacaman, M. J. *Nanotechnology.* **2005**, *16* (10), 2346–2353. https://doi.org/10.1088/0957-4484/16/10/059.

15. Ayala-Nunez, N. V.; Villegas, H. H. L.; Turrent, L. C. I.; Padilla, C. R. *J. Nanobiotechnol.* **2009***, 5*, 2–9. doi: 10.1007/s12030-009-9029-1)

16. Yacamán, M. J.; Ascencio, J. A.; Liu, H. B.; Gardea-Torresdey, J. *J. Vac. Sci. Technol.* **2001**, *19* (4), 1091. https://doi.org/10.1116/1.1387089.

17. Gao, M. J.; Sun, L.; Wang, Z. Q.; Zhao, Y. B.; *Mat. Sci. Eng. C Mater.* **2013**, *33*, 397–404.

18. Hong, X.; Wen, J.; Xiong, X.; Hu, Y. *Environ. Sci. Pollut. Res.* **2016**, *23*, 4489–4497.

19. Zheng, X.; Huang, H.; Su, Y.; Wei, Y.; Chen, Y. *Water Sci. Technol.* **2015**, *72* (1), 99–105. https://doi.org/10.2166/wst.2015.194

20. He, S.; Feng, Y.; Ni, J.; Sun, Y.; Xue, L.; Feng, Y.; Yu, Y.; Lin, X.; Yang, L. *Chemosphere.* **2016**, *147*, 195–202. https://doi.org/10.1016/j.chemosphere.2015.12.055.

21. Wang, J.; Shu, K.; Zhang, L.; Si, Y. *Pedosphere* **2017**, *27* (3), 482–490. https://doi.org/10.1016/s1002-0160(17)60344-8.

22. Chavan, S.; Nadanathangam, V. *Agronomy.* **2019**, *9* (3), 140. https://doi.org/10.3390/agronomy9030140.

23. Courtois, P.; Rorat, A.; Lemiere, S.; Guyoneaud, R.; Attard, E.; Levard, C.; Vandenbulcke, F. *Environ. Pollut.* **2019**, *253*, 578–598. https://doi.org/10.1016/j.envpol.2019.07.053.

24. Wu, L.; Zhu, G.; Zhang, X.; Si, Y. Sci. Total Environ. 2020, 706, 135711–135711. https://doi.org/10.1016/j.scitotenv.2019.135711.

25. Mujeebur, R. K.; Fromm, K. M.; Tanveer F. R.; Giese, B.; Ahamad, F.; Turner, R. J.; Füeg, M.; Marsili, E. *Part Part Syst Charact.* **2020**, *37* (5), 1900419–1900419. https://doi.org/10.1002/ppsc.201900419.

26. Wang, L.; Hu, C.; Shao, L. *Int. J. Nanomedicine.* **2017**, *12*, 1227–1249. https://doi.org/10.2147/ijn.s121956.

27. Rahmatpour, S.; Shirvani, M.; Mosaddeghi, M. R.; Nourbakhsh, F.; Bazarganipour, M. *Geoderma.* **2017**, *285*, 313–322. https://doi.org/10.1016/j.geoderma.2016.10.006.

28. Awet, T. T.; Kohl, Y.; Meier, F.; Straskraba, S.; Grün, A.-L.; Ruf, T.; Jost, C.; Drexel, R.; Tunc, E.; Emmerling, C. *Environ. Sci. Eur.* **2018**, *30* (1). https://doi.org/10.1186/s12302-018-0140-6.

29. Shan, J.; Li, X.; Yang, K.; Weijun X.; Wen, Q.; Zhang, Y.; Lihui Y.; Weng, L.; Teng, Z.; Wang, L. *ACS Nano.* **2019**, *13* (12), 13797–13808. https://doi.org/10.1021/acsnano.9b03868.

30. Bondarenko, L. S.; Kovel, E. S.; Kydralieva, K. A.; Dzhardimalieva, G. I.; Illés, E.; Tombácz, E.; Kicheeva, A. G.; Kudryasheva, N. S. *Nanomater.* **2020**, *10* (8), 1499. https://doi.org/10.3390/nano10081499.

31. Yan, C.; Huang, J.; Cao, C.; Li, R.; Ma, Y.; Wang, Y. *Environ. Sci. Pollut. Res*.**2020**, *27* (8), 8058–8070. https://doi.org/10.1007/s11356-019-07347-5.

32. Taş, A.; Keklikcioğlu Çakmak, N.; Agbektaş, T.; Zontul, C.; Özmen, E.; Siliğ, Y. *Scientific Journal of Mehmet Akif Ersoy University*, **2020**, *3* (3), 77-83.

33. Kolesnikov, S. I.; Timoshenko, A.; Minnikova, T.; Tsepina, N. I.; Kazeev, K.; Yuliya Akimenko, V.; Zhadobin, A.; Shuvaeva, V.; Rajput, V. D.; Mandzhieva, S.; Sushkova, S.; Minkina, T.; Dudnikova, T.; Mazarji, M.; El Sabagh, A.; Siddiqui, M. H.; Kumar Singh, R. *Plants* **2021**, *10* (10), 2080–2080. https://doi.org/10.3390/plants10102080.

34. Grün, A.-L.; Emmerling, C. *Environ. Sci. Eur.* **2018**, *30* (1). https://doi.org/10.1186/s12302-018-0160-2.

35. Porter, A. E.; Gass, M.; Muller, K.; Skepper, J. N.; Midgley, P. A.; Welland, M. E. *Nat. Nanotechnol* **2007**, *2* (11), 713–717. https://doi.org/10.1038/nnano.2007.347.

36. Shrivastava, S.; Bera, T.; Roy, A.; Dash, D. *Nanotechnology.* **2007**, *18* (22), 225103.

37. Yang, W.; Shen, C.; Ji, Q.; An, H.; Wang, J.; Liu, Q.; Zhang, Z. *Nanotechnol.* **2009**, *20* (8), 085102. https://doi.org/10.1088/0957-4484/20/8/085102.

38. Gomes, E.; de Souza, A. R.; Orjuela, G. L.; Da Silva, R.; de Oliveira, T. B.; Rodrigues, A. *Fungal Biol.* **2016**, 459–492. https://doi.org/10.1007/978-3-319-27951-0_21.

39. Mehta, R.; Singhal, P.; Singh, H.; Damle, D.; Sharma, A. K. *3 Biotech* **2016**, *6* (1). https://doi.org/10.1007/s13205-016-0368-z.

40. Dumorne, K.; Cordova, D. C.; Astorga-Elo, M.; Renganathan, P. *J. Microbiol. Biotechnol.* **2017**, *27* (4), 649–659. https://doi.org/10.4014/jmb.1611.11006.

41. Hasnaa R.; Temsaah, A. F.; Azmy, M.R.; Amr E. A.; Walaa, G. H. *J. Pure Appl. Microbiol.* **2018**; *12*(4):1687-1702. https://dx.doi.org/10.22207/JPAM.12.4.02.

42. Ayisa, T. T.; Oyedokun, N. O.; Ideh, R.; Itoroabasi, J. O.; Ideh, R. R.; Egbi, T. K.; Ahmadu, J. H.; Orji, S. L. *African J. Sci. Technol. Res.* **2022**, 4 (1), 63-70.

43. Özdemir; S.; Kılınç, E.; Poli, A.; Nicolaus, B.; Güven, K. *J. Chem. Eng.* **2009**, *152* (1), 195–206. https://doi.org/10.1016/j.cej.2009.04.041.

44. Özdemir; S.; Kılınç, Poli, A.; Nicolaus, B.; Güven, K. *World J Microbiol Biotechnol.* **2012**, *28* (1), 155–163. https://doi.org/10.1007/s11274-011-0804-5.

45. Alkan, H.; Gul-Guven, R.; Guven, K.; Erdogan, S.; Dogru, M. *Pol. J. Environ. Stud.* **2015**, *24*, 1903–1910. https://doi.org/10.15244/pjoes/36359.

46. Koul, B.; Chaudhary, R.; Taak, P. In *Microbe Mediated Remediation of Environmental Contaminants* **2021**, (pp. 115-128). Woodhead Publishing. https://doi.org/10.1016/B978-0-12-821199-1.00012-2.

47. Gul Guven, R.; Guven, K.; Poli, A.; Nicolaus, B. *Enzyme Microb.* **2007**, *40(6)*, 1570-1577.

48. Gul Guven, R.; Kaplan, A.; Guven, K.; Matpan, F.; Doğru, M. *Biotechnol. Bioprocess Eng.* **2011**, *16(1)*, 114-119.

49. Matpan Bekler, F.; Stougaard, P.; Guven, K.; Gul Guven, R.; Acer, O. *Cell. Mol. Biol.* **2015**, *61(3)*, 71-78.

50. Matpan Bekler, F.; Yalaz, S.; Acer, O.; Guven, K. *Fresenius Environ. Bull.* **2017**, *26(3)*, 2251-2259.

51. Tunç, Ş.; Maptan Bekler, F.; Güven, K. *Biotech Studies*, **2021**, *30(2)*, 71-78.

52. Dong, F.; Valsami-Jones, E.; Kreft, JU. *J Nanopart Res.* **2016**, *18*, 259. https://doi.org/10.1007/s11051-016-3565-0.

53. Matpan Bekler, F.; Yalaz, S.; Guven, K.; Gul Guven, R.; 3. International Eurasian Conference on Biological and Chemical Sciences (EurasianBioChem 2020) 19-20 April **2020** Ankara / Turkey. Proceeding Book pp:132-139.

54. Matpan Bekler, F.; Yalaz, S.; Güven K. *Rom. Biotechnol. Lett.* **2018**, *23(5)*, 13964-13975.

55. Matpan Bekler, F.; Yalaz, S.; Gul Guven, R.; Guven, K. (2019). *J. Serb. Chem. Soc.* **2019**, *84(10)*, 1093–1104.

56. Guven, K.; Togrul, S.; Uyar, F.; Ozant, S.; De Pomerai, D. I. *Enzyme Microb.* **2003**, *32* (6), 658–664. https://doi.org/10.1016/s0141-0229(03)00025-5.

57. Guven, K.; Yolcu, M.; Gul-Guven, R.; Erdogan, S.; Pomerai, D. D. *Cell Biol. Toxicol.* **2005**, *21* (2), 73–81. https://doi.org/10.1007/s10565-005-0123-4.

58. Khan, I.; Saeed, K.; Khan, I. *Arabian J Chem.* **2017**, *12* (7). https://doi.org/10.1016/j.arabjc.2017.05.011.

59. Ameen, F.; Alsamhary, K.; Alabdullatif, J. A.; ALNadhari, S. *Ecotoxicol. Environ. Saf.* **2021**, *213*, 112027. https://doi.org/10.1016/j.ecoenv.2021.112027

60. Seol J.W.; Hur, T.Y.; Jung, Y.H.; Kang, S.J.; Park, S.Y. *J Vet Clin* **2010,** 27, 252–256.

61. Sintubin, L.; De Gusseme, B.; Van der Meeren, P. *Appl Microbiol Biotechnol*, **2011**, 91, 153–162. https://doi.org/10.1007/s00253-011-3225-3.

62. Zhang, L.; Wu, L.; Si, Y.; Shu, K. *PLoS One* **2018**, 13, No. e0209020.

63. Ahmed, B.; Ameen, F.; Rizvi, A.; Ali, K.; Sonbol, H.; Zaidi, A.; Khan, M. S.; Musarrat, J. *ACS Omega* **2020**, *5* (14), 7861–7876. https://doi.org/10.1021/acsomega.9b04084.

64. Dakal, T. C.; Kumar, A.; Majumdar, R. S.; Yadav, V. *Front. Microbiol.* **2016**, *7*. https://doi.org/10.3389/fmicb.2016.01831.

65. Dovbeshko, G. *Talanta* **2000**, *53* (1), 233–246. https://doi.org/10.1016/s0039-9140(00)00462-8.

66. Hou, Y.C.; Zhao, P.; Zhang, F.; Yang, S.; Rady, A.; Wijewardane, N. K.; Huang, J.; Li, M. *Food Sci. Technol.* **2022**, *42*. https://doi.org/10.1590/fst.100821.

67. Mordechai S.; Sahu, R.; Hammody, Ziad.; Mark, S.; Kantarovich, K.; Guterman, H.; A. Podshyvalov; Goldstein, J.; Argov S. *J. Microsc.* **2004**, *215* (1), 86–91. https://doi.org/10.1111/j.0022-2720.2004.01356.x.

68. Nandiyanto, D.; Riezqa Andika; Aziz, M.; Lala Septem Riza. *Indones. J. Sci. Technol.* **2018**, *3* (2), 82–82. https://doi.org/10.17509/ijost.v3i2.12752.

69. Brisebois, P. P.; Arnold, A. A.; Chabre, Y. M.; Roy, R.; Marcotte, I. *Eur. Biophys. J.* **2012**, *41* (6), 535–544. https://doi.org/10.1007/s00249-012-0809-5.

70. Jackson, M.; Sowa, M.G.; Mantsch, H.H. *Biophys. Chem.* **1997**, *68*, 109–125.

71. Szalontai, B.; Nishiyama, Y.; Gombos, Z.; Murata, N. *Biochim. Biophys. Acta (BBA)-Biomembr.* **2000**, *1509*, 409–419.

72. Banyay, M.; Sarkar, M.; Gräslund, A. *Biophys. Chem.* **2003**, *104*, 477–488.

73. Saraeva, I.; Tolordava, E.; Yushina, Y.; Sozaev, I.; Sokolova, V.; Khmelnitskiy, R.; Sheligyna, S.; Pallaeva, T.; Pokryshkin, N.; Khmelenin, D.; et al. *Nanomaterials* **2022**, *12*, 3857

74. Azim, A. A.; Aksel, H.; Zhuang, T.; Mashtare, T.; Babu, J. P.; Huang, G. T.J. *J. Endod.* **2016**, *42* (6), 928–934. https://doi.org/10.1016/j.joen.2016.03.009.

75. Javvaji, P. K.; Dhali, A.; Francis, J.; Kolte, A. P.; Mech, A.; Roy, S. C.; Mishra, A.K.; Bhatta, R. *Front. Cell Dev. Biol.* **2020**, *8*. https://doi.org/10.3389/fcell.2020.00764.

76. Kalyanaraman, B.; Darley-Usmar, V.; Davies, K. J. A.; Dennery, P. A.; Forman, H. J.; Grisham, M. B.; Mann, G. E.; Moore, K.; Roberts, L. J.; Ischiropoulos, H. *Free Radic. Biol. Med.* **2012**, *52* (1), 1–6. https://doi.org/10.1016/j.freeradbiomed.2011.09.030.

77. Patlolla, A. K.; Hackett, D.; Tchounwou, P. B. *Mol. Cell. Biochem.* **2014**, *399* (1-2), 257–268. https://doi.org/10.1007/s11010-014-2252-7.

78. Gan J.; Sun, J.; Chang, X.; Li, W.; Li, J.; Niu, S.; Kong, L.; Zhang, T.; Wu, T.; Tang, M.; Xue, Y. *J Appl Toxicol.* **2020**, *40* (6), 815–831. https://doi.org/10.1002/jat.3946.

79. Kim, S.; Lee, H.-S.; Ryu, D.-S.; Young Choi, S.; Lee, D.-S. *Korean J. Microbiol. Biotechnol.* **2011**, *39* (1), 77–85.

80. Wu, D.; Fan, W.; Kishen, A.; Gutmann, J. L.; Fan, B. *J. Endod.* **2014**, *40* (2), 285–290. https://doi.org/10.1016/j.joen.2013.08.022.

81. Matpan Bekler, F.; Yalaz, S.; Gul Guven, R.; Acer, O.; Guven, K. *The Online J. Sci. Technol.* **2018**, *8(2),* 32-38.

82. Yalaz, S.; Matpan Bekler, F.; Acer, O. (2019). *Banat's J. Biotechnol.* **2019**, *10(19),* 42-50.

83. Acer, Ö.; Matpan Bekler, F. *Turk. J. Nature Sci.* **2021**, *10(1),* 130-136.

84. Jung, W. K.; Koo, H. C.; Kim, K. W.; Shin, S.; Kim, S. H.; Park, Y. H. *Appl. Environ. Microbiol.* **2008**, *74* (7), 2171–2178. https://doi.org/10.1128/aem.02001-07.

85. Rai, M. K.; Deshmukh, S. D.; Ingle, A. P.; Gade, A. K. *J. Appl. Microbiol.* **2012**, *112* (5), 841–852. https://doi.org/10.1111/j.1365-2672.2012.05253.x.

86. Holt, K.B.; Bard, A.J. *Biochemistry.* **2005,** *44,*13214–13223.

87. You, C,; Han, C,; Wang, X,; Zheng, Y,; Li, Q,; Hu, X,; Sun, H. *Mol. Biol. Rep.* **2012**, *39* (9), 9193-201. doi: 10.1007/s11033-012-1792-8.

88. Pareek, V.; Gupta, R.; Panwar, J. *Mater. Sci. Eng. C.* **2018**, *90*, 739–749. https://doi.org/10.1016/j.msec.2018.04.093.

89. Tang, S.; Zheng, J. *Adv. Healthc. Mater.* **2018**, *7* (13), 1701503. https://doi.org/10.1002/adhm.201701503.

90. Sondi, I.; Salopek-Sondi, B. *J. Colloid Interface Sci.* **2004**, *275* (1), 177–182. https://doi.org/10.1016/j.jcis.2004.02.012.

91. Ahmad, A.; Wei, Y.; Syed, F.; Tahir, K.; Rehman, A. U.; Khan, A.; Ullah, S.; Yuan, Q. *Microb. Pathog.* **2017**, *102*, 133–142. https://doi.org/10.1016/j.micpath.2016.11.030.